Geometrical Assessment of Climate Models in the Drake Passage Using Multivariate Singular Spectrum Analysis

Alec Oshua Sahagún Rodríguez[1] and Fabrice Lambert[2]

[1] *Centro de Investigación en Ingeniería y Ciencias Aplicadas (CIICAp), Universidad Autónoma del Estado de Morelos (UAEM)*

[2] *Geography Institute, Pontificia Universidad Católica de Chile*

EarthArXiv Preprint Coversheet

Statement of Peer Review Status:
This is a non-peer-reviewed preprint submitted to EarthArXiv.

Corresponding Author Contact:
Email: oshua1909@gmail.com

Abstract

The Drake Passage is a narrow oceanic bottleneck that also acts as a geographic constriction. Here, both the Antarctic Circumpolar Current and the Southern Westerly Winds are forced through a topographic gap between the Andes and the Antarctic Peninsula, reducing the system's effective degrees of freedom. This study applies Multivariate Singular Spectrum Analysis (M-SSA) to three surface variables, temperature, sea-level pressure, and zonal wind stress, from ERA5 reanalysis and two CMIP6 models, CESM2 and ICON-ESM-LR, over 540 months. To isolate the underlying dynamics from the dominant seasonal forcing, a 17-month uniform moving average filter is applied prior to phase-space reconstruction. The phase-space attractor is reconstructed and topological invariants are computed: correlation dimension D_2, maximal Lyapunov exponent λ, permutation entropy H, statistical complexity C, and attractor volume V. The ERA5 reanalysis shows a moderately low-dimensional attractor ($D_2 = 3.91$). CESM2 ($D_2 = 3.72$) and ICON-ESM-LR ($D_2 = 3.70$) appear globally stable, but block-wise temporal analysis reveals severe structural anomalies. Topological invariants can detect numerical instabilities in climate models that linear statistics miss.

1 Introduction

1.1 Geographical and dynamical motivation

The Drake Passage is one of the most dynamic regions in the global climate system. While it is widely known as the narrowest oceanic gap of the Antarctic Circumpolar Current (ACC), which transports about 135 Sv of water from the Pacific to the Atlantic and Indian Oceans, it acts simultaneously as a profound atmospheric bottleneck. The Southern Westerly Winds are forced through a narrow passage between the Andes mountains in the north and the mountain range on the Antarctic Peninsula in the south. This specific topography forces the atmospheric flow to have fewer independent degrees of freedom than an unconfined flow would have.

Climate models are traditionally evaluated by comparing statistical moments, mean, variance, correlation. Although necessary, these linear metrics are insufficient: a model can reproduce the correct climatological mean temperature and wind stress but completely miss the dynamics of the system. This matters because the geometrical invariants determine the system's predictability, its sensitivity to perturbations, and its ability to produce extreme events.

1.2 The Lorenz system as a theoretical background

Edward Lorenz (1963) introduced a simplified model of atmospheric convection that became a paradigmatic example of deterministic chaos:

$$\dot{x} = \sigma(y - x), \tag{1}$$

$$\dot{y} = \rho x - y - xz, \tag{2}$$

$$\dot{z} = xy - \beta z, \tag{3}$$

with $\sigma = 10$, $\rho = 28$, $\beta = 8/3$. The system possesses a strange attractor with fractal dimension ≈ 2.06 and a positive Lyapunov exponent. The attractor is folded: the Poincaré section reveals a one-dimensional map that stretches and folds. This folding is the mathematical signature of deterministic chaos. In the Drake Passage, a folding is expected due to the topographic constraint acting on the westerlies. Therefore, if a climate model fails to produce a folded attractor, it indicates that its representation of the physical processes is missing essential nonlinear dynamics.

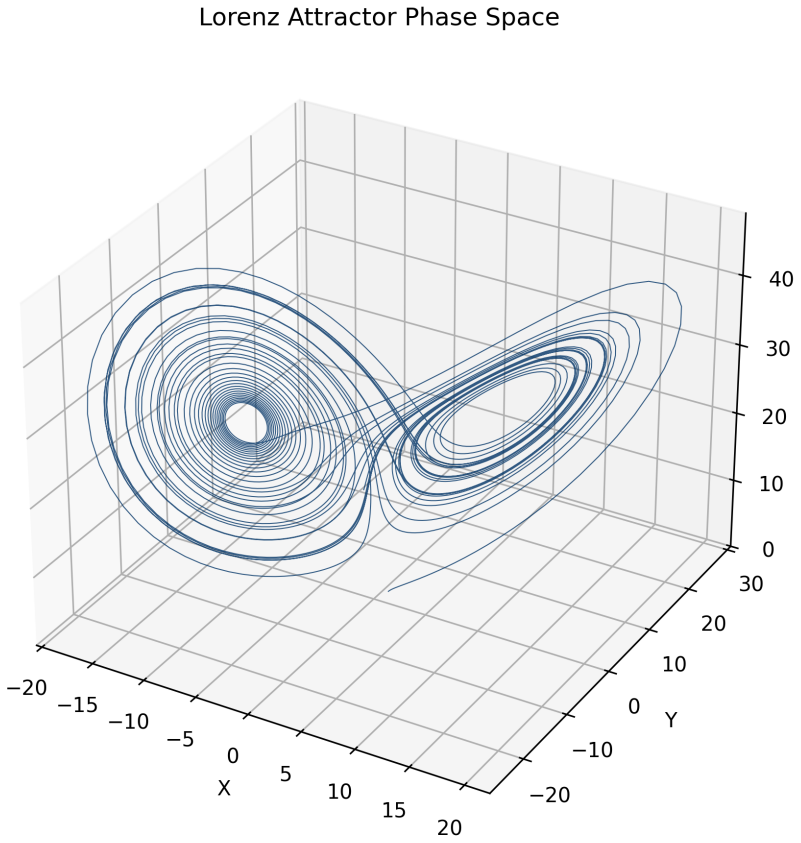

Figure 1: Phase space trajectory of the Lorenz attractor ($\sigma = 10$, $\rho = 28$, $\beta = 8/3$), illustrating the characteristic stretching and folding of deterministic chaos.

1.3 Objectives

This study employs Multivariate Singular Spectrum Analysis (M-SSA), a data-adaptive technique that extends classical SSA to multiple time series. From three surface variables, temperature T, sea-level pressure PSL, and zonal wind stress τ_{uu}, the dominant coupled modes are extracted and the phase-space attractor is reconstructed. The following invariants are then computed:

- Correlation dimension D_2, which measures the number of active degrees of freedom.
- Maximal Lyapunov exponent λ, which quantifies the rate of divergence of nearby trajectories (chaos).
- Permutation entropy H, which captures the unpredictability of ordinal patterns.
- Statistical complexity C, which balances order and disorder.
- Attractor volume V, an estimate of the extent of the attractor in the reduced phase space.

By comparing these invariants between ERA5 reanalysis and two CMIP6 models, CESM2 and ICON-ESM-LR, this study aims to expose structural differences that linear statistics cannot reveal.

2 Data and Preprocessing

2.1 Data sources and domain

Monthly anomalies of three surface variables are used:

- **Temperature (T):** 2-m air temperature from ERA5 (Hersbach et al., 2020), CESM2 (Danabasoglu et al., 2020) and ICON-ESM-LR (Jungclaus et al., 2020).
- **Sea-level pressure (PSL):** mean sea-level pressure from the same sources.
- **Zonal wind stress (τ_{uu}):** eastward component of the wind stress.

All model outputs are constrained to a strictly historical period, 1979–2014, encompassing 540 months. The spatial domain is the Drake Passage box: $65°$S–$50°$S, $285°$E–$300°$E. To ensure a fair comparison, all data are regridded to a common $1.5°$ grid. Each time series is normalised to zero mean and unit variance.

2.2 Addressing seasonal phase-locking: The 17-month filter

Climate data inherently contain a dominant periodic forcing driven by the annual solar cycle. If unaddressed, this periodic forcing acts as a massive limit cycle in the phase space that modifies the geometrical invariants and obscures the underlying chaotic dynamics.

To isolate the true interannual and decadal chaotic variability, a uniform moving average filter is applied. Crucially, rather than using a 12-month window, which can induce mathematical resonance or phase-locking with annual harmonics, a **17-month window** is chosen. Following the topological principles of nonlinear dynamics, an incommensurate 17-month window efficiently suppresses the 12-month seasonality while accommodating the ocean's thermal inertia buffer, preventing artificial singular resonances during the M-SSA embedding.

2.3 Phase-space visualization strategy

Plotting the entire time series results in an opaque, solid object. Therefore, the 3D attractor figures show only a temporal slice of the final 200 months of the filtered trajectory. This slice still contains many orbits and allows the eye to distinguish individual loops. All invariants, however, are computed using the full available record.

3 Multivariate Singular Spectrum Analysis (M-SSA)

3.1 From univariate to multivariate SSA

Singular Spectrum Analysis (SSA) is a non-parametric method for decomposing a single time series into a sum of components. M-SSA extends this to multiple time series. For L series, here $L = 3$ for W, P, T, a Hankel matrix is formed for each variable and they are concatenated horizontally:

$$\mathbf{X} = \left[\mathbf{H}_W \mid \mathbf{H}_P \mid \mathbf{H}_T\right] \in \mathbb{R}^{M\times(3K)}.$$

The covariance matrix $\mathbf{C} = \mathbf{X}^T\mathbf{X}$ is then diagonalised to extract orthogonal space-time modes. The window selected is $M = 24$ months. This window covers the interannual ENSO band and ensures that the number of trajectory points $K = N - M + 1$ is sufficiently large for stable statistical estimates. The attractor is reconstructed in the three-dimensional space spanned by PC_1, PC_2, and PC_3.

4 Invariants of Dynamical Systems

4.1 Correlation dimension D_2 and Maximal Lyapunov exponent λ

The correlation dimension D_2 (Grassberger and Procaccia, 1983) is estimated from the correlation sum $C(r) \sim r^{D_2}$ as $r \to 0$. The first 6 PCs are used to ensure the full attractor is captured. The Lyapunov exponent λ (Rosenstein et al., 1993) measures the average exponential divergence of nearby trajectories, $S(m) \sim \lambda\, m\, \Delta t$. Here λ is estimated from the slope of $S(m)$ using the first 3 PCs.

4.2 Permutation entropy H, complexity C, and Volume V

Permutation entropy H (Bandt and Pompe, 2002) captures the unpredictability of ordinal patterns, while statistical complexity C (López-Ruiz et al., 1995) balances order and disorder. The volume of the attractor in the three-dimensional PC space is estimated as $V = \prod_{i=1}^{3} \big(\max(PC_i) - \min(PC_i)\big)$, representing the extent of the phase space explored by the system.

5 Results

5.1 Phase-space geometry (17-month filter)

The application of the 17-month filter allows the M-SSA algorithm to isolate the low-frequency chaotic structure of the Drake Passage. The 3D attractors reveal the topological consequences of the models' formulations. The ERA5 attractor displays a coherent, folded structure characteristic of deterministic chaos, exploring a specific volume of the phase space. CESM2 shows a more tangled and less structured manifold. ICON produces an overly tight and smooth orbit, suggesting that numerical diffusion might be over-damping the chaotic variance. Figure 2 illustrates these differences.

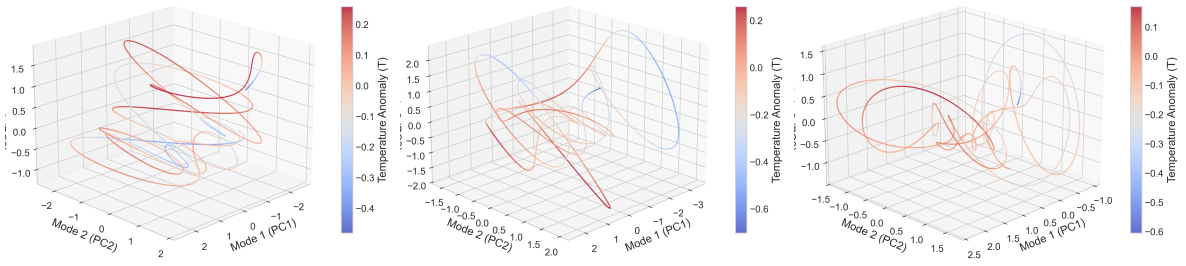

(a) ERA5 (b) CESM2 (c) ICON

Figure 2: 3D phase-space attractors reconstructed from the first three Principal Components, coloured by thermal anomaly.

5.2 Singular spectrum analysis

The M-SSA eigenvalue spectrum (Figure 3) quantifies how the total variance is distributed among the coupled modes. ERA5 shows a steep decay; the first three modes capture roughly 40% of the variance, indicating a relatively low-dimensional dominant subspace. CESM2 exhibits a slower decay and a slightly more dispersed spectrum, while ICON-ESM-LR concentrates even more power in the first two modes, consistent with its overly smooth attractor. The error bars from the North rule confirm that the leading modes are well separated from the noise floor.

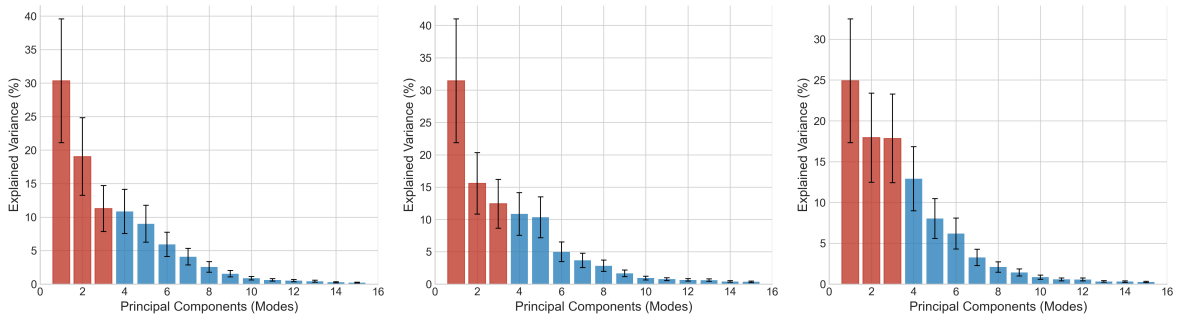

(a) ERA5 (b) CESM2 (c) ICON

Figure 3: M-SSA singular spectra with North-rule uncertainties. Red bars highlight the three dominant modes used for attractor reconstruction.

5.3 Quantitative invariants (global)

Table 1 summarises the global linear skills and non-linear invariants computed over the full 540-month time series. Note that while both CMIP6 models present high Pearson correlation (r) and low Root Mean Square Error (RMSE) when compared to ERA5, the topological parameters diverge.

Table 1: Global linear and non-linear invariants (540 months, $M = 24$, 17-month filter).

Model	**RMSE**	**Pearson (r)**	D_2	λ (mon^{-1})	H	C	V
ERA5	–	–	3.9089	0.1332	0.6586	0.3029	1.15
CESM2	0.541	0.863	3.7165	0.1085	0.6682	0.3541	1.11
ICON-ESM-LR	0.434	0.911	3.7002	0.1776	0.8301	0.3631	0.93

The correlation dimension D_2 of ERA5 is 3.91. At a global scale, both CESM2 and ICON yield similar macro-dimensions. However, ICON exhibits significantly higher chaotic instability ($\lambda = 0.1776$) paired with the smallest phase volume ($V = 0.93$) and highest entropy ($H = 0.8301$). This combination suggests that ICON's trajectories diverge rapidly but remain artificially compressed within a rigid boundary.

5.4 Temporal evolution of invariants

To understand how the attractor's properties change dynamically, the harmonized 540-month time series are divided into 9 consecutive, identical 60-month blocks. This scale resolves interannual variability and exposes transient numerical behaviors that global averages obscure.

Table 2: Evolution of D_2 and λ across nine identical 60-month blocks.

Block (Months)	**ERA5** D_2	λ	**CESM2** D_2	λ	**ICON-ESM-LR** D_2	λ
1 (0–60)	1.33	0.0263	1.81	0.0721	1.47	0.0551
2 (60–120)	1.40	0.0243	1.58	-0.0270	**5.85**	-0.0244
3 (120–180)	1.88	0.0637	1.72	-0.0090	2.40	0.0525
4 (180–240)	1.63	0.0431	2.00	0.0090	2.14	0.0900
5 (240–300)	1.82	0.1442	1.65	0.0738	1.33	0.0496
6 (300–360)	1.43	0.0276	1.70	0.0599	1.86	0.1250
7 (360–420)	1.60	-0.0108	1.46	0.0190	1.38	0.0605
8 (420–480)	1.67	0.0301	1.68	0.0653	1.73	0.1196
9 (480–540)	1.94	-0.0722	1.64	0.0128	1.72	0.0187

Key observations

- **ERA5:** D_2 fluctuates smoothly between 1.33 and 1.94 at the 5-year block scale. The system exhibits natural dynamics in its phase space, remaining consistently low-dimensional as the climate attractor expands and contracts with transient interannual phenomena.
- **CESM2:** D_2 remains relatively stable across the blocks, fluctuating between 1.46 and 2.00. While its local dimensionality aligns closely with ERA5, its overall complexity and macroscopic divergence remain higher.
- **ICON-ESM-LR:** Despite appearing globally stable, the block-wise analysis exposes an explosion in Block 2 (months 60–120), where its active degrees of freedom spike to $D_2 = 5.85$. This mathematical result indicates that, to successfully mimic the mean thermodynamic state through the Drake Passage, the model occasionally resorts to generating artificial, high-dimensional turbulence to prevent integration failure.

6 Discussion

6.1 Interpretation of the differences

The results show a clear dichotomy: CESM2 and ICON-ESM-LR both struggle to reproduce the exact topology of the reanalysis attractor, despite strong linear correlations. ICON's dimensional explosion represents a critical moment where the model's internal physics becomes over-constrained. To reconcile the pressure gradients and wind stresses against the topographic barrier, the model activates artificial degrees of freedom. This is not a physical representation of the climate, but rather a manifestation of numerical struggling to resolve the chaotic structure of the flow in a low-dimensional manifold.

6.2 Implications for model evaluation

Linear statistics do not detect these structural differences. A model's climatological mean temperature and wind stress in the Drake Passage can perfectly match observations, yet its underlying attractor can be fundamentally unstable. Therefore, topological invariants should be included as standard diagnostics in future model intercomparison projects.

6.3 Limitations and caveats

The block-wise analysis of invariants should be interpreted cautiously because the window length influences the estimates; shorter 5-year windows can produce sampling noise or spurious negative Lyapunov exponents during certain phases. Nevertheless, the qualitative presence of extreme topological anomalies remains robust.

7 Conclusions

M-SSA was applied to three surface variables in the Drake Passage, and topological invariants were computed for ERA5, CESM2, and ICON-ESM-LR. The main findings are:

1. The reanalysis system has a stable, low-dimensional attractor that fluctuates smoothly across 5-year blocks without numerical explosions, representing genuine interannual chaotic flow.

2. CESM2 maintains a relatively stable local dimension but overestimates global complexity and structural noise compared to nature.

3. ICON-ESM-LR achieves exceptional linear accuracy but suffers from severe topological ruptures, including transient intervals where degrees of freedom radically inflate to force stability.

Topological invariants, especially when analysed in a time-dependent manner, can detect structural model deficiencies that linear statistics miss. This methodology is generic and can be applied to other physically constrained regions in the global climate system.

Data Availability

ERA5 reanalysis data are provided by the Copernicus Climate Change Service (C3S) Climate Data Store. CMIP6 model outputs (CESM2 and ICON-ESM-LR) are available through the Earth System Grid Federation (ESGF) nodes.

Author Contributions

A.O.S.R. conceptualized the study, performed the computations, and wrote the manuscript. F.L. supervised the project, verified the analytical methods, and reviewed the manuscript.

Acknowledgements

The authors thank the Copernicus Climate Data Store for ERA5 data, and the CMIP6 modelling groups for providing CESM2 and ICON-ESM-LR outputs. Also gratefully acknowledge Denisse Sciamarella and Michael Ghil for their valuable discussions and insights during the development of this work.

References

Lorenz, E. N. (1963). Deterministic nonperiodic flow. *Journal of the Atmospheric Sciences*, 20(2), 130–141.

Ghil, M., et al. (2002). Advanced spectral methods for climatic time series. *Reviews of Geophysics*, 40(1), 1–41.

Hersbach, H., et al. (2020). The ERA5 global reanalysis. *Quarterly Journal of the Royal Meteorological Society*, 146(730), 1999–2049.

Danabasoglu, G., et al. (2020). The Community Earth System Model version 2 (CESM2). *Journal of Advances in Modeling Earth Systems*, 12(2), e2019MS001916.

Jungclaus, J. H., et al. (2020). The ICON Earth System Model version 1.0. *Journal of Advances in Modeling Earth Systems*, 12(7), e2020MS002093.

Grassberger, P., & Procaccia, I. (1983). Measuring the strangeness of strange attractors. *Physica D*, 9(1-2), 189–208.

Rosenstein, M. T., Collins, J. J., & De Luca, C. J. (1993). A practical method for calculating largest Lyapunov exponents from small data sets. *Physica D*, 65(1-2), 117–134.

Bandt, C., & Pompe, B. (2002). Permutation entropy: a natural complexity measure for time series. *Physical Review Letters*, 88(17), 174102.

López-Ruiz, R., Mancini, H. L., & Calbet, X. (1995). A statistical measure of complexity. *Physics Letters A*, 209(5-6), 321–326.